10ème Congrès Français d'Acoustique

Lyon, 12-16 Avril 2010

Direct computation of the noise radiated by a propulsive jet at a Mach number of 3.3

N. de Cacqueray[1], C. Bogey[1] and C. Bailly[1]

[1] Laboratoire de Mecanique des Fluides et d'Acoustique, 36 Av Guy De Collongue 69134 Ecully Cedex

{nicolas.cacqueray, christophe.bogey, christophe.bailly}@ec-lyon.fr

A high supersonic, shocked and heated jet at a Reynolds number of 10^5 is computed by large-eddy simulations (LES) to directly determine its radiated sound field, using low-dissipation schemes in combination with an adaptative shock-capturing method. The jet exit parameters are a Mach number of $M_e = u_e/c_e = 3.30$, a static pressure of $P_e = 0.5 \times 10^5$ Pa and a static temperature of $T_e = 360$ K, where u_e and c_e are the exit velocity and sound speed. The aerodynamic and the near acoustic fields are compared with to theoretical results[1] and experimental data.[2–4]Some insights into the far acoustic field are finally shown.

1 Introduction

In supersonic jets, large turbulent scales are wellknown to play an important role in noise generation.[5] They could especially radiate noise by Mach wave mechanisms in the shear layer,[3,6,7] by interacting with the shock-cell structure[8,9] and by non-linear effects at the end of the potential core.[10,11] However, few experimental[4,12,13] and computational[14,15] studies exist for high Mach number jets and the importance of the different noise mecanisms has not yet been identified clearly.

Over the past ten years, the development of low-dissipation and low-dispersion numerical schemes[16–18] has permitted to carry out Direct Noise Computation (DNC) on high Reynolds subsonic jets to compute its radiated sound field[19,20] and to analyze noise sources.[21] However, the computation of the noise radiated by supersonic jets using low-dissipation methods is still a challenging problem. Nevertheless, a DNC without shock-capturing scheme was successfully applied to an underexpanded planar jet at a fully expanded Mach number of $M_j = 1.55$ in order to investigate screech generation.

In the present study, DNC using low-dissipation methods is applied to a high Mach number, heated and shocked jet to compute its acoustic field and to investigate noise sources. The computation of the flow and the radiated sound fields is performed using compressible large eddy simulation (LES). Then, acoustic near-field quantities are propagated to the far-field from a control surface using Euler equations.

The outline of the paper is the following. In the first section, the numerical procedure and the simulation parameters are presented. In the second section, the mean aerodynamic field is then examined. Finally, near-field and far-field acoustic results are shown in the third part.

2 Numerical Procedure

2.1 Simulation parameters

In the present work, an overexpanded jet at an exit Mach number of $M_e = 3.30$, an exit temperature of $T_e = 360$ K and an exit static pressure of $p_e = 0.5 \times 10^5$ Pa, originating at $z = 0$ from a pipe nozzle of length $0.5r_e$ where r_e is the nozzle radius, is considered. The stagnation pressure p_0 and temperature T_0 are 28.6×10^5 Pa and 1144 K. The equivalent fully expanded conditions defined from the stagnation conditions and a static pressure of $p_j = 10^5$ Pa are a Mach number of $M_j = 2.83$ and a temperature of $T_j = 439$ K. The acoustic Mach number M_a defined as the ratio of the fully expanded velocity u_j over the ambient sound speed c_∞ is equal to 3.47. The Reynolds number Re estimated from the exit quantities is equal to 0.94×10^5. At the inlet, a Blasius profile for a laminar boundary layer of thickness $\delta = 0.05r_e$ is imposed for the mean velocity and a Crocco-Busemann profile is used for the mean density. Random pressure disturbances of low amplitude are introduced in the nozzle, yielding nozzle-exit maximum velocity fluctuations of 0.3% of the jet velocity.

The jet exit quantities are similar to those of an experiment performed at LEA Poitiers on MARTEL facility.[4] However, due to numerical limitations, the Reynolds number of the simulation is 20 times smaller than the Reynolds number in the experiment.

2.2 Numerical methods

The simulations are performed by solving the unsteady compressible Navier-Stokes equations in cylindrical coordinates,[22] using low-dispersion and low-dissipation finite-difference schemes.[18,23] The numerical treatement of Mohseni & Colonius[24] is used for the jet centerline singularity and the simulation time step is increased by reducing the azimuthal resolution near the jet axis.[25] The LES approach is based on the explicit application of a selective filtering to the flow variables[26] to take into account the dissipative effects of the subgrid scales. Non-reflective acoustic boundary conditions[27] are implemented for radial and upstream boundaries. A sponge zone is used downstream to avoid acoustical reflections at the outflow boundary.[27] It has been successfully implemented in previous LES of subsonic round jets[21,28] and of a supersonic rectangular jet.[8] An adaptative and conservative shock-capturing scheme is used to remove Gibbs oscillations near shocks.[29] The grid used for the present jet contains $n_r \times n_\theta \times n_z = 256 \times 128 \times 840 = 28 \times 10^6$ points, and 120,000 iterations carried out using NEC SX - 8 computers are necessary to ensure statistical convergence. In the radial direction, the mesh is refined down to $\Delta r = 0.0072 r_e$ at the nozzle lip to have an accurate resolution of the shear layer. In the axial direction, the grid is streched downstream of $z = 52 r_e$ to implement the sponge zone. To compute far-field noise spectra and directivities, the LES near-field obtained on a control surface located at $r = 9.5 r_e$ is propagated to 50 radii from the nozzle exit, by solving the Euler equations with the shock capturing scheme[29] on a grid of $561 \times 128 \times 1001 = 72 \times 10^6$ points. the mesh size is constant and equal to $\Delta r_{acou} = 0.1 r_e$ in the radial direction and to $\Delta z_{acou} = 0.074 r_e$ in the axial direction. The numerical cut-off Strouhal number is thus $St_c = 2 f_c r_e / U_e = 1.37$ where $f_c = c_\infty / (4 \Delta r_{acou})$.

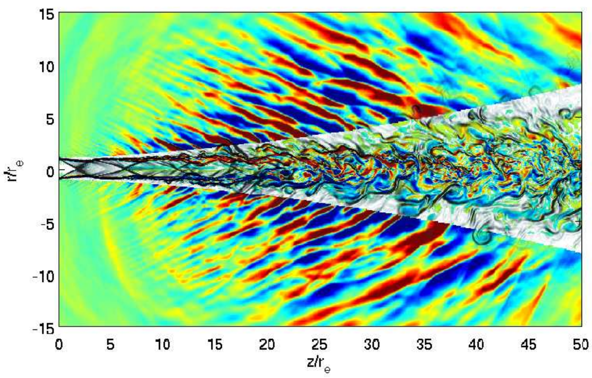

Figure 1: Snapshots in the (z, r) plane of density gradient norm $\nabla\rho$ in gray scale, of azimuthal vorticity ω_θ in color scale in the jet and of fluctuating pressure p' in color scale outside the jet. The color scale ranges for levels from -5000 to 5000 Pa for p'.

3 Aerodynamic results

3.1 Instantaneous field

Snapshot of azimuthal vorticity ω_θ, of density gradient norm $\nabla\rho$ and of fluctuating pressure field is shown in figure 1. The distances are made dimensionless with respect to the nozzle radius r_e. Shock cells and temperature fronts are visible using the density gradient. The development of the turblence in the shear layer and turbulent mixing after the jet potential core can be observed. Vorticity due to shock interactions[30] can also be noticed in the potential core close to the jet axis. The acoustic waves radiate mainly in the downstream direction and Mach waves are visible attached to the shear layer. Low-amplitude waves can also be seen in the upstream direction.

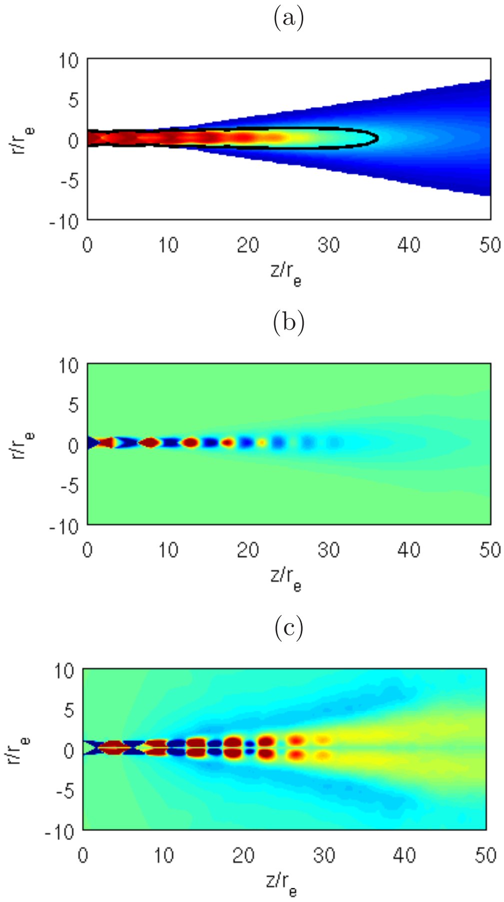

Figure 2: Representation in the (z, r) plane of (a) mean axial velocity $< u_z >$, of (b) mean static pressure $< p >$ and of (c) mean radial velocity $< u_r >$. The color scales range for levels from 80 to 1255 m/s for $< u_z >$, from 0.5×10^5 to 1.5×10^5 Pa for $< p >$ and from -30 to 30 m/s for $< u_r >$. The sonic line is plotted in black on the mean axial velocity field.

3.2 Mean flow features

The fields of mean axial velocity $< u_z >$, mean static pressure $< p >$ and mean radial velocity $< u_r >$ are presented in figure 2. The sonic line corresponding to an axial Mach number $M_z = < u_z > / c$ equal to 1, where c is the local sound speed, is also plotted in figure 2(a). The sonic core length is thus $L_s = 36 r_e$. As expected, a shock-cell structure is observed on the mean pressure field in figure 2(b) due to the adaptation of the jet exit conditions to the ambient field. Shock cells could also be noticed on the mean radial velocity colormap in figure 2(c). Outside the flow field, the negative radial velocity is linked to the jet axial development.
The variations of the inverse of the centerline velocity u_{axis} is plotted in figure 3. Data are made dimensionless according to the jet exit conditions. The end of the potential core L_c is located around $z = 20 r_e$, which is in fair agreement with numerical results from Nonomura & Fujii.[14,15] Moreover, data obtained at MARTEL experimental facility[4] with similar exit conditions, but with a higher Reynolds number, display the end of the potential core around 24 radii and the end of the sonic core around 50 radii which compare roughly with the present computation.
In perfectly expanded self-similarity jets, mean center-

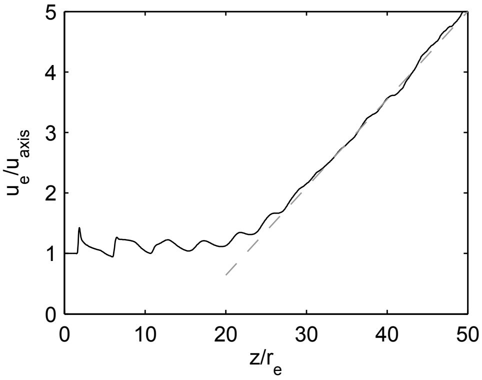

Figure 3: Variations along the jet centerline of the inverse of the mean longitudinal velocity u_{axis}: ——— present computation, − − − line to evaluate the similarity parameter.

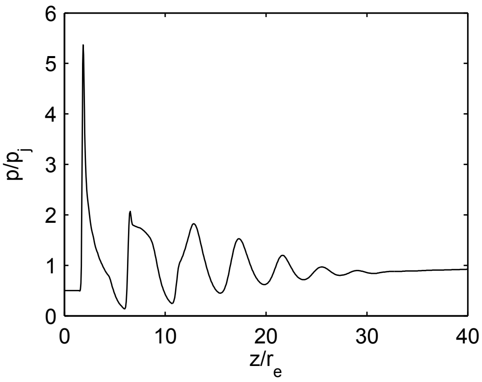

Figure 4: Variations of the mean static pressure $< p >$ along the jet centerline.

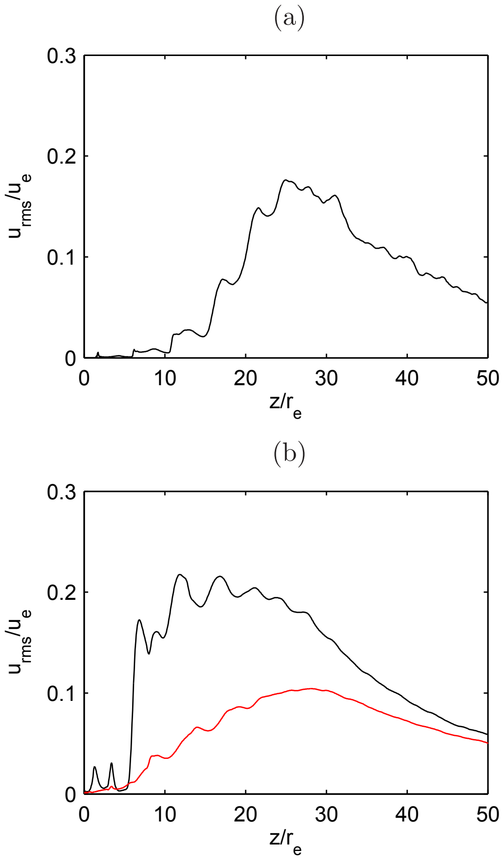

Figure 5: Variations of rms velocity fluctuations: (a) ——— axial velocity fluctuations along the jet centerline, and (b) ——— axial velocity fluctuations ——— radial velocity fluctuations along the line $r = r_j$.

line velocity u_{axis} is indeed given by:

$$\frac{u_{axis}}{u_j} = A \frac{2r_j}{z - z_0} \qquad (1)$$

where u_j and r_j are the fully expanded velocity and radius, A is the decay constant and z_0 denotes the virtual origin. In the present simulation, $A = 4.90$ is found if fully expanded quantities are used and A is equal to 3.44 if exit conditions are used. For unheated jets,[31] A is usually between 5 and 6.5. The discrepancies between the velocity decays from the present simulation and the literature may come from temperature and Mach number effects[32,33] or from changes in the initial boundary layer thickness.[22,34] The variations of the centerline mean static pressure $< p >$ are plotted in figure 4, where six shock-cells are noticed. The static pressure after the first shock on the jet centerline can be estimated using straight shock formula. A pressure of 6.3×10^5 Pa is found, which is in agreement with the simulation results in figure 4. In the present computation, the average shock-cell length L_{shock} is equal to $4.6r_e$. The average shock-cell length could also be estimated using the formula of Tam and Tanna[9]:

$$L_{shock} = 2\pi(M_j^2 - 1)^{1/2} r_j / \mu_1 \qquad (2)$$

where r_j is the fully expanded radius and $\mu_1 = 2.40483$. Using equation 2, it is found $L_{shock} = 5.6r_e$. The shock-cell spacing provided by the computation appears to be smaller than expected by the formula of Tam and Tanna.[9] This trend might be due to the fact that the estimation of Tam and Tanna[9] does not consider the shear-layer thickness.[8,35,36]

3.3 Turbulent flow properties

Root-mean-square (rms) variations of the axial velocity along the jet centerline and of the axial and radial velocities along the line $r = r_j$ are plotted in figure 5. The maximum of rms velocity along the jet axis is reached after the end of the potential core. Along the line $r = r_j$, the peak of the radial fluctuating velocity is also obtained at the end of the potential core. However, the maximum of the rms axial velocity in the shear layer is located before the end of the potential core and axial velocity fluctuations are nearly constant between $z = 13r_e$ and $z = 20r_e$.

4 Acoustic results

4.1 Acoustic near-field

All the acoustic results have been computed with a reference pressure of 2×10^{-5} Pa. The overall sound pressure level (OASPL) at a distance of 9.5 radii from the jet centerline is compared to experimental data from Greska *et al.*[2] in figure 6. The experimental jet is fully-expanded, with an exit Mach number M_j of 2 and a ratio of stagnation temperature over ambient

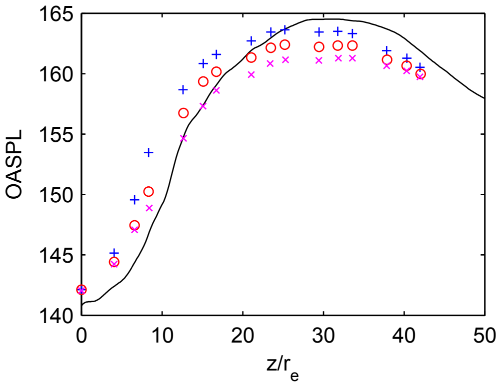

Figure 6: Variations of the overall sound pressure level (OASPL) in the axial direction. ——— Present computation at $r = 9.5r_e = 11.8r_j$, measurements of Greska *et al.*[2]: × at $r = 12r_j$, o at $r = 10r_j$ and + at $r = 8r_j$.

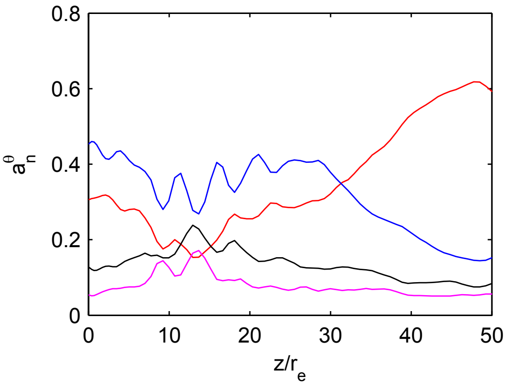

Figure 7: Variations in the axial direction of the coefficients a_n^θ obtained from the azimuthal decomposition of cross-correlation R^θ of fluctuating pressure at $r = 9.5r_e$: ——— $n = 0$, ——— $n = 1$, ——— $n = 2$ and ——— $n = 3$

temperature of 4. The OASPL of the present simulation is in fair agreement with experimental data provided at $r = 8r_j$, $10r_j$ and $12r_j$, where r_j is the jet radius. The variation of the peak location might be due to a difference of potential core length between simulation and experiment.

The cross-correlation function R^θ of the fluctuating pressure p' at point (r, θ, z) is defined by:

$$R^\theta(\delta\theta) = \frac{< p'(\theta)p'(\theta + \delta\theta >}{< p'^2(\theta) >^{1/2} < p'^2(\theta + \delta\theta) >^{1/2}} \qquad (3)$$

where $\delta\theta$ is the azimuthal separation. The cross-correlation function R^θ obtained along the line $r = 9.5r_e$ is then decomposed into a Fourier sum[37] as follows:

$$R^\theta(\delta\theta) = \sum_{n=0}^{\infty} a_n^\theta \cos(n\delta\theta) \qquad (4)$$

where a_n^θ is the relative amplitude of the Fourier mode n. The coefficients of the axisymmetric mode, $n = 0$, and of the three modes, $n = 1, 2, 3$, along the line $r = 9.5r_e$ are presented in figure 7. Distinct behaviors are noticed. Before $z = 31r_e$, the mode $n = 1$ dominates the near acoustic field and downstream of $z = 31r_e$, the axisymmetric mode $n = 0$ has the highest amplitude. Finally, around $z = 13r_e$, the acoustic field appears to be less correlated, and the modes $n = 2$ and $n = 3$ cannot be neglected.

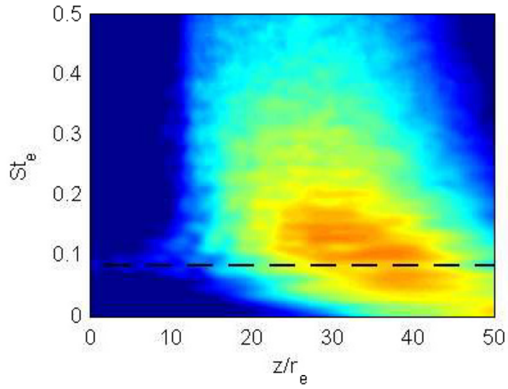

Figure 8: Variations in the axial direction of the power spectral density (PSD) of the fluctuating pressure at $r = 9.5r_e$. The color scale ranges for levels from 150 to 180 dB. – – – Estimation of the screech frequency according to Tam *et al.*.[1]

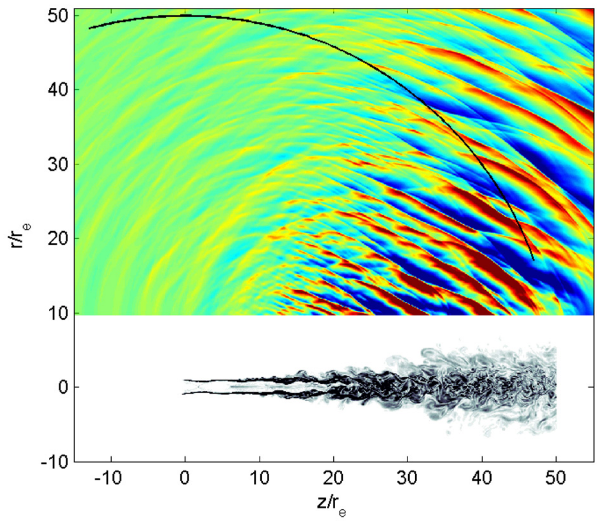

Figure 9: Snapshots in the (z, r) plane of the vorticity in the jet and of the fluctuating pressure propagating using Euler equations. The color scale ranges for levels from -3000 to 3000 Pa for the fluctuating pressure. ——— Recorded data at $r = 50r_e$.

The variations of the power spectral density (PSD) of the fluctuating pressure along the line $r = 9.5r_e$ are shown in figure 8 as a function of the Strouhal number $St_e = 2r_ef/u_e$. A maximum is observed downstream of $z = 20r_e$, between $St_e = 0.03$ and $St_e = 0.2$. However, a peak is noticed in the upstream direction. The peak frequency corresponds to the screech frequency predict by Tam *et al.*.[1]

4.2 Acoustic far-field

The LES near-field obtained on a control surface located at $r = 9.5r_e$ is now propagated to 50 radii from the nozzle exit using Euler equations in combination with the adaptative shock-capturing scheme.[29] A snapshot of acoustic pressure is shown in figure 9. Acoustic waves propagate mainly in the downstream direction, but shock-associated noise is noticed in the upstream direction. The power spectral density of the acoustic pressure is presented in figure 10 as a function of the Strouhal number St_e and of the angle of observation in the downstream direction θ. The origin is taken at the nozzle exit. A maximum of acoustic radiation is observed from $\theta = 20°$ and $\theta = 40°$ and between $St_e = 0.03$ and $St_e = 0.2$. The peak frequency of the broadband shock-associated noise f_{shock} is estimated by the model of Tam & Tanna[9]:

$$f_{shock} = \frac{u_c}{L_{shock}(1 - M_c \cos(\theta))} \quad (5)$$

where u_c is the convection velocity taken equal to $0.7u_j$ for axisymmetric jets and $M_c = u_c/c_\infty$ is the convective Mach number. The frequency predicted by the model of Tam & Tanna[9] is plotted in figure 10 but it is not in good agreement with the simulation. However, it can be noticed in figure 5 that the maximum of the axial velocity fluctuations is located far from the nozzle exit between the third and the fifth shock. The origin of the shock-associated noise model[9] is then modified and taken at the fourth shock at $z = 17r_e$. The frequency predicted by the model with a modified origin is also plotted in figure 10 and is in fair agreement with computed data.

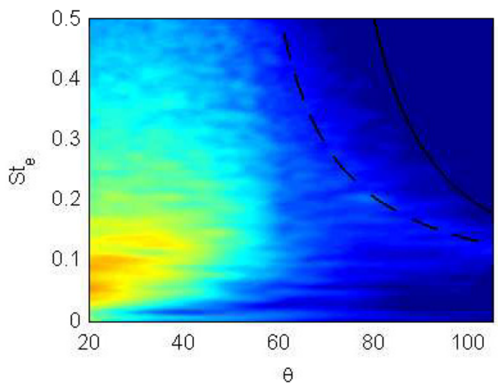

Figure 10: Colormap of the power spectral density of the fluctuating pressure in the far-field as a function of the Strouhal number St_e and of the angle of observation θ. The color scale ranges for levels from 140 to 180 dB. Prediction of the central frequency of shock associated noise given by equation 5: ——— without origin correction and – – – with origin correction.

5 Conclusion

Direct Noise Computation has been performed for a high Mach number heated jet using compressible large-eddy simulation. The mean flow field and the near acoustic field level have been characterized.

The jet radiates mainly in the downstream direction between $St_e = 0.03$ and $St_e = 0.2$. However a peak frequency corresponding to the screech frequency predicted by Tam *et al.*[1] is found in the upstream direction. A more detailed analysis is needed to clearly identify the role of the different noise mechanisms[5] on the acoustic spectra. This study could be possible by using far-field analysis, linear stability theory,[3] correlations[10,21] and cross-spectra.[8]

Acknowledgments

The first author is grateful to the Centre National d'Etudes Spatiales (CNES) for financial support. This work was granted access to the HPC resources of IDRIS under the allocation 2009-020204 made by GENCI (Grand Equipement National de Calcul Intensif).

References

[1] Tam, C., Seiner, J. and Yu, J., "Proposed relationship between broadband shock associated noise and screech tones," *Journal of Sound and Vibration*, Vol. 110, No. 2, 1986, pp. 309-321.

[2] Greska, B., Krothapalli, A., Horne, W. and Burnside, N., "A near-field study of high temperature supersonic jets," AIAA Paper 2008-3026, 2008.

[3] Seiner, J., Bhat, T. and Ponton, M., "Mach wave emission from high-temperature supersonic jet," *AIAA Journal*, Vol. 32, No. 12, 1994, pp. 2345-2350.

[4] Varnier, J. and Gély, D., "Caractérisation aérodynamique et acoustique d'un jet fortement supersonique en présence d'un obstacle plan," RT 112/3643, 1998.

[5] Tam, C., "Supersonic jet noise," *Annu. Rev. Fluid Mech.*, Vol. 27, 1995, pp. 17-43.

[6] McLaughlin, D.K., Morrison, G.L. and Troutt, T.R., "Experiments on instability waves in a supersonic jet and their acoustic radiation," *Journal of Fluid Mechanics*, Vol. 69, 1975, pp. 73-95.

[7] Krothapalli, A., Arakeri, V. and Greska, B., "Mach wave radiation: a review and an extension," AIAA Paper 2003-1200, 2003.

[8] Berland, J., Bogey, C. and Bailly, C., "Numerical Study of screech generation in a planar supersonic jet," *Physics of Fluids*, Vol. 19, No. 7, 2007.

[9] Tam, C.K.W., and Tanna, H.K., "Shock associated noise of supersonic jets from convergent-divergent nozzles," *Journal of Sound and Vibration*, Vol. 81, No. 3, 1982, pp. 337-357.

[10] Panda, J. and Seasholtz, R.G., "Experimental investigation of density fluctuations in high-speed jets and correlation with generated noise," *Journal of Fluid Mechanics*, Vol. 450, 2002, pp. 97-130.

[11] Tam, C.K.W., Viswanathan, K., Ahuja, K.K. and Panda, J., "The sources of jet noise: experimental evidence," *Journal of Fluid Mechanics*, Vol. 615, 2008, pp. 253-292.

[12]Seiner, J., Ponton, M., Jansen, B. and lagen, N. “The effects of temperature on supersonic jet noise emission,” AIAA/DLR Paper 92-02-046, 1992.

[13]Krothapalli, A., Greska, B. and Wishart D., “Aeroacoustics of a heated Mach 2.0 Jet,” AIAA Paper 2005-2931, 2005.

[14]Nonomura, T. and Fujii K., “Over-expansion effects on Mach 3.0 supersonic jet acoustics,” AIAA Paper 2008-2836, 2008.

[15]Nonomura, T. and Fujii K., “Mach number and temperature effects on Mach wave emission from supersonic jets,” AIAA Paper 2008-6587, 2008.

[16]Tam, C. and Webb, J., “Dispersion-relation-preserving finite difference schemes for computational aeroacoustics,” *J. Comput. Phys.*, Vol. 103, 1992, pp. 16-42.

[17]Tam, C. and Webb, J., “Dispersion-relation-preserving finite difference schemes for computational aeroacoustics,” *J. Comput. Phys.*, Vol. 107, No. 2, 1993, pp. 262-281.

[18]Bogey, C. and Bailly, C., “A family of low dispersive and low dissipative explicit schemes for flow and noise computations,” *J. Comput. Phys.*, Vol. 194, No. 1, 2004, pp. 194-214.

[19]Bogey, C. and Bailly, C., “Computation of high Reynolds number jet and its radiated noise using large eddy simulation based on explicit filtering,” *Computer and Fluids*, Vol. 35, No. 10, 2006, pp. 1344-1358.

[20]Bodony, D.J. and Lele S.K., “Current status of jet noise predictions using large-eddy simulation,” *AIAA Journal*, Vol. 46, No. 2, 2008.

[21]Bogey, C. and Bailly, C., “An analysis of the correlations between the turbulent flow and the sound pressure field of subsonic jets,” *Journal of Fluid Mechanics*, Vol. 583, 2007, pp. 71-97.

[22]Bogey, C. and Bailly, C., “Influence of the nozzle-exit boundary-layer thickness on the flow and acoustic fields of initially laminar jets,” AIAA Paper 2009-3409, 2009.

[23]Berland, J.,Bogey, C., Marsden, O. and Bailly, C., “High-order, low dispersive and low dissipative explicit schemes for multi-scale and boundary problems,” *J. Comput. Phys.*, Vol. 224, No. 2, 2007, pp. 637-662.

[24]Mohseni, K. and Colonius, T., “Numerical treatment of polar coordonate singularities,” *J. Comput. Phys.*, Vol. 157, 2000, pp. 787-795.

[25]Bogey, C., de Cacqueray, N. and Bailly, C., “Finite differences for coarse azimuthal discretization and for reduction of effective resolution near origin of cylindrical flow equations,” *submitted to J. Comput. Phys.*.

[26]Bogey, C. and Bailly, C. “Turbulence and energy budget in a self-preserving round jet: direct evaluation using large-eddy simulation,” *Journal of Fluid Mechanics*, Vol. 627, 2009, pp. 129-160.

[27]Bogey, C. and Bailly, C. “Three-dimensional non-reflective boundary conditions for acoustic simulations: far field formulation and validation test cases,” *Acta Acustica United with Acustica*, Vol. 8, 2002, pp. 463-471.

[28]Bogey, C. and Bailly, C., “Large Eddy Simulations of transitional round jets: influence of the Reynolds number on flow development and energy dissipation,” *Physics of Fluids*, Vol. 18, No. 6, 2006, pp. 1-14.

[29]Bogey, C., de Cacqueray, N. and Bailly, C., “A shock capturing methodology based on adaptative spatial filtering for high-order non-linear computations,” *J. Comput. Phys.*, Vol. 228, No. 5, 2009, pp. 1447-1465.

[30]Hornung, H. and Schwendeman, D., “Oblique shock reflection from an axis of symmetry: shock dynamics and relation to the Guderley singularity,” *Journal of Fluid Mechanics*, Vol. 438, 2001, pp. 231-245.

[31]Hussein, H.J., Capp, S.P. and George, W.K., “Velocity measurement in a high-Reynolds-number, momentum-concerving, axisymmetric, turbulente jet,” *Journal Fluid Mechanics*, Vol. 258, 1994, pp. 31-75.

[32]Lau, J.C. , “Effect of exit Mach number and temperature on mean-flow and turbulence characteristics in round jets,” *Journal Fluid Mechanics*, Vol. 105, 1981, pp. 193-218.

[33]Bartosiewicz, Y., Mercadier, Y. and Proulx, P., “Numerical investigations on dynamics and heated transfer in a turbulent underexpanded jet,” *AIAA Journal*, Vol. 40, No. 11, 2002, pp. 2257-2265.

[34]Bodony, J.D. and Lele, S.K., “Low-frequency sound sources in high-speed turbulent jets,” *Journal of Fluid Mechanics*, Vol. 617, 2008, pp. 231-253.

[35]Morris, P.J., Bhat, T.R.S. and Chen, C., “A linear shock cell model for jets of arbitrary exit geometry,” *Journal of Sound of Vibration*, Vol. 132, No. 2, 1989, pp. 199-211.

[36]Jothi, T.J.S and Srinivasan, K., “Role of initial conditions on noise from underexpanded pipe jets,” *Physics of Fluids*, Vol. 21, 2009.

[37]Bogey, C. and Bailly, C., “Influence of nozzle-exit boundary layer conditions on the flow and acoustic fields of initially laminar jets,” *submitted to J. Fluid Mech.*, 2010.